History force on coated microbubbles propelled by ultrasound

Valeria Garbin,[1] Benjamin Dollet,[1,a)] Marlies Overvelde,[1] Dan Cojoc,[2] Enzo Di Fabrizio,[2,b)] Leen van Wijngaarden,[1] Andrea Prosperetti,[1,c)] Nico de Jong,[1,d)] Detlef Lohse,[1] and Michel Versluis[1]

[1]*Physics of Fluids Group and Research Institute for Biomedical Technology BMTI, University of Twente, 7500 AE Enschede, The Netherlands*
[2]*CNR-INFM, Laboratorio Nazionale TASC, 34149 Trieste, Italy*

In this paper the unsteady translation of coated microbubbles propelled by acoustic radiation force is studied experimentally. A system of two pulsating microbubbles of the type used as contrast agent in ultrasound medical imaging is considered, which attract each other as a result of the secondary Bjerknes force. Optical tweezers are used to isolate the bubble pair from neighboring boundaries so that it can be regarded as if in an unbounded fluid and the hydrodynamic forces acting on the system can be identified unambiguously. The radial and translational dynamics, excited by a 2.25 MHz ultrasound wave, is recorded with an ultrahigh speed camera at 15×10^6 frames/s. The time-resolved measurements reveal a quasisteady component of the translational velocity, at an average translational Reynolds number $\langle \mathrm{Re}_t \rangle \approx 0.5$, and an oscillatory component at the same frequency as the radial pulsations, as predicted by existing models. Since the coating enforces a no-slip boundary condition, an increased viscous dissipation is expected due to the oscillatory component, similar to the case of an oscillating rigid sphere that was first described by Stokes ["On the effect of the internal friction of fluids on the motion of pendulums," Trans. Cambridge Philos. Soc. **9**, 8 (1851)]. A history force term is therefore included in the force balance, in the form originally proposed by Basset and extended to the case of time-dependent radius by Takemura and Magnaudet ["The history force on a rapidly shrinking bubble rising at finite Reynolds number," Phys. Fluids **16**, 3247 (2004)]. The instantaneous values of the hydrodynamic forces extracted from the experimental data confirm that the history force accounts for the largest part of the viscous force. The trajectories of the bubbles predicted by numerically solving the equations of motion are in very good agreement with the experiment. © 2009 American Institute of Physics.
[doi:10.1063/1.3227903]

I. INTRODUCTION

Bubbles in a sound wave translate unsteadily under the action of an effective force $F_G(t) = -V(t) \nabla p(t)$, where $V(t)$ is the volume and $\nabla p(t)$ is the local instantaneous pressure gradient. In a sound wave $\nabla p(t)$ is oscillatory and the bubble volume $V(t)$ pulsates, resulting in a force known as acoustic radiation force, which periodically changes both direction and magnitude.[1] The corresponding motion of the bubble is an oscillatory translation, at the frequency of the radial pulsations, around a position that slowly drifts. The time average of the acoustic radiation force $F_{\mathrm{Bj}} = -\langle V(t) \nabla p(t) \rangle$, the so-called Bjerknes force, is nonzero and results in the net translation of a bubble. If the sound wave driving such motion is the secondary wave emitted by a neighboring pulsating bubble, a mutual interaction comes into effect and two bubbles pulsating in phase attract each other. The average force is then called secondary Bjerknes force.

The translation of uncoated bubbles due to acoustic radiation forces has been the subject of numerous studies over the past decades, only a few of which are mentioned here. Crum and Eller[2] and Crum[3] validated expressions for the primary and secondary Bjerknes forces against experimental data by measuring the mean terminal velocity of millimeter-sized bubbles. Good agreement of a time-averaged equation of motion with experiment was found by balancing the Bjerknes force with a quasisteady drag force. Indeed, flow oscillations have no effect on the mean terminal velocity if the governing equations can be linearized. According to the analysis of Landau and Lifshitz,[4] for a sphere of radius R oscillating with frequency ω and amplitude a, the convective term $(v \cdot \nabla)v$ is of order $\omega^2 a^2/R$, and therefore it can be neglected compared to $\partial v/\partial t \sim \omega^2 a$ for oscillations of small amplitude, $a \ll R$, which appears to be the case in the experiments of Crum and Eller[2] and Crum.[3] Oğuz and Prosperetti[5] developed an approximate formulation for the instantaneous dynamics of two interacting bubbles to investigate the influence of nonlinear effects. From numerical calculations, a richer behavior was found than what was predicted by the linear theory of Bjerknes forces, although viscous effects were neglected. Reddy and Szeri,[6] in a numerical study on

a)Present address: Institut de Physique de Rennes, CNRS/Université Rennes 1, 35042 Rennes, France.
b)Present addresses: Laboratorio BIONEM, Università "Magna Græcia" di Catanzaro, 88100 Germaneto, Italy and Nanobiotech Laboratory, Italian Institute of Technology, 16163 Genova, Italy.
c)Also at Department of Mechanical Engineering, The Johns Hopkins University, Baltimore, Maryland 21218, USA.
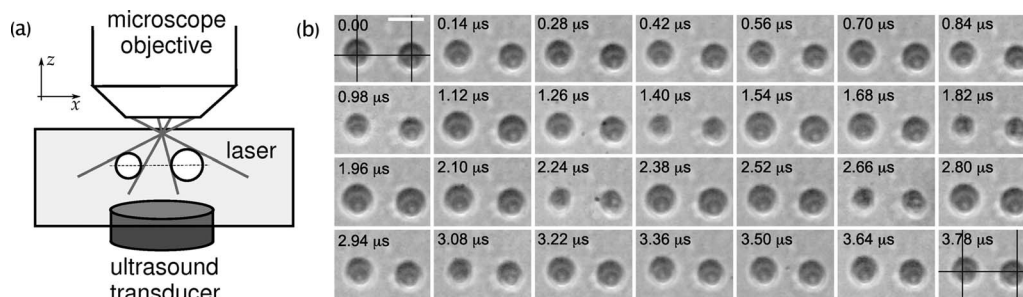d)Also at Erasmus Medical Center, 3000 Rotterdam, The Netherlands.

FIG. 1. Observations of the dynamics of two coated bubbles in ultrasound. (a) Layout of the experiment (side view). A microscope objective is used to focus the laser traps (optical tweezers) and for transmission imaging. The direction of incidence of the ultrasound beam is orthogonal to the line of centers x. (b) Frames from an ultrahigh speed time series of bubble dynamics (top view). The recording is taken at 13.4×10^6 frames/s, corresponding to an interframe time of 70 ns. Here only every second frame is shown. The black crosses in the first and last frames indicate the initial positions of the bubble centers. The distance between the bubbles decreases due to the secondary Bjerknes force. White scale bar: 5 μm (enhanced online).[URL: http://dx.doi.org/10.1063/1.3227903.1]

the propulsion of microbubbles by traveling ultrasound waves, included viscous effects through the expression obtained by Magnaudet and Legendre[7] for shear-free bubbles with time-dependent radius. The history force was found to be unimportant, consistent with the criterion given in Ref. 7 that it plays a role only if at least one of the two Reynolds numbers, Re_t and Re_r, is smaller than 1. Here $Re_t = R|U|/\nu$ is the Reynolds number for the translation and $Re_r = R|\dot{R}|/\nu$ is the one for the radial dynamics.

History force effects have been shown to be important for shear-free bubbles, for instance, in single bubble sonoluminescence.[8] It is well known that the history force on a rigid sphere is much larger than on a shear-free sphere,[9] and surfactant molecules adsorbed on the surface of a bubble change the shear-free boundary condition to a no-slip one.[10] For the oscillatory motion of a rigid sphere, an increased viscous dissipation is to be expected since the vorticity remains confined in an oscillatory boundary layer of thickness $\delta \sim \sqrt{\omega/\nu}$, where ω is the frequency of the oscillations and ν is the kinematic viscosity of the liquid. The Basset history integral[11] generalizes to an arbitrary velocity the expression for the drag on an oscillating sphere that was first obtained by Stokes.[12] Stokes' solution for an oscillating sphere was also found by Mei[13] to reproduce the numerical solution of the full Navier–Stokes equation in the limit of high frequency of oscillations. An expression for the history force on a no-slip bubble with time-dependent radius was derived and validated experimentally by Takemura and Magnaudet[14] at finite Re_t.

Bubbles whose surface is immobilized by surfactants are encountered in a number of contexts and they have proven particularly beneficial in ultrasound medical imaging. In this application, contrast enhancement is obtained by injecting in the blood vessels microscopic gas bubbles,[15] ranging in size from 1 to 5 μm, coated by design with a surfactant monolayer to stabilize them against dissolution. Several models have been proposed to describe the effect of a coating on the radial dynamics of a pulsating microbubble.[16–19] In contrast, its influence on the markedly unsteady translation in an ultrasound field has hardly been treated. Emerging applications of contrast agent microbubbles in drug delivery and targeted molecular imaging[20–22] demand a deeper understanding of the behavior on the time scale of competing phenomena, for

instance, the binding to target molecules or the interaction with the blood vessel walls. These applications ultimately require a detailed description of the *instantaneous* translation of *coated* microbubbles. The first experimental study on the instantaneous translation of contrast agent microbubbles in a traveling ultrasound wave, by Dayton *et al.*,[23] compared time-resolved optical observations with a dynamical model which included a finite-Reynolds-number empirical extension of the quasisteady drag on a no-slip bubble. The authors observed that such a model systematically overpredicted the total displacement and ascribed the discrepancy to the fact that in the experiment, the bubbles were in contact with the top wall of the sample chamber due to buoyancy, with the attendant difficulty of quantifying the friction coefficient between a bubble and the wall.

The purpose of the present paper is to provide a time-resolved description of the unsteady translation of coated microbubbles propelled by ultrasound. We consider a system of two bubbles translating due to their mutual radiation force, which offers the advantage that the pressure gradient on one bubble is known with great accuracy from the time-resolved observations of the radial and translational dynamics of the neighboring bubble. We predict the trajectories of the two bubbles with the aid of the measured radial dynamics and investigate the influence of the history force in a range of parameters (bubble size R_0, viscosity of the fluid ν, frequency ω, and relative radial excursion $\Delta R/R_0$) of interest for medical ultrasound imaging.

II. EFFECT OF CONFINING GEOMETRY: MICROMANIPULATION OF BUBBLES

Isolating bubbles from the walls of the container greatly simplifies the problem of determining the forces acting on them. Here we use optical tweezers to position bubbles at a prescribed distance from the sample chamber wall. The experimental technique is described in Sec. III. As sketched in Fig. 1(a), a bubble pair is pushed downward and away from the wall, with the line of centers parallel to the wall. The bubbles can be held in the prescribed position for the

duration of the experiment. We therefore avoid the problem, encountered by Dayton *et al.*,[23] of sliding friction at the wall.

The influence of a rigid wall on the flow field can be modeled in the inviscid case through the method of images. The wall is replaced by a virtual particle, which mirrors the dynamics of the real particle and generates a flow that, by canceling out the primary flow, satisfies the zero normal velocity condition at the wall. In our experiments the sample chamber wall is not perfectly rigid; for a partially transparent wall the following considerations do not strictly hold, but the effect of a rigid wall can be considered as a limiting case.

The quasisteady drag F_{QS} for a sphere translating near a rigid boundary can be written as $F_{QS} = -6\pi\eta\gamma RU$, where γ is Faxén's correction factor. Up to third order in the parameter R/r, where R is the sphere radius and r is the distance from the boundary, one has[24] $\gamma = [1 - 9/16(R/r) + 1/8(R/r)^3]^{-1}$. For $R/r \sim 1/20$, the typical value in our experiments, the drag is increased by less than 5%.

The image of a pulsating bubble also generates a spherical wave, with the result that an acoustic radiation force arises between the bubble and the wall through the coupling of the bubble and its image. The acoustic radiation force between pulsating bubbles is derived in Sec. IV. The leading term depends on $(R/r)^2$, and therefore for $R/r \sim 1/20$ the net attraction force to the wall becomes negligible. Incidentally, this force acts in a direction orthogonal to the line of centers [see Fig. 1(a)] and would not affect the force balance in the direction of interest.

By positioning the bubbles at least 20 radii away from the wall, we therefore minimize the effect of reflections on the translational dynamics so that the bubbles can be regarded as if in an unbounded liquid. In eliminating these disturbances we can focus on the forces acting on the bubbles purely due to the interaction with the liquid.

III. EXPERIMENTAL PROCEDURE

The facilities and protocols used in this study to simultaneously control the experimental conditions with optical tweezers and optically record the dynamics of microbubbles in ultrasound have been presented previously.[25] The optical tweezers setup was based on an upright microscope (Olympus) modified to couple a laser beam into a water-immersed $100\times$ objective lens (Olympus, numerical aperture NA = 1). A strongly focused Gaussian beam is known to produce a three-dimensional optical trap for dielectric microparticles with a refractive index greater than the surrounding medium. Since a bubble has a lower refractive index than the surrounding liquid, a suitable optical trap consists in this case of a laser beam exhibiting a minimum of intensity on the optical axis, such as a Laguerre–Gaussian beam.[26] We produced the intensity distribution required to generate two traps by converting a 1064 nm continuous-wave linearly polarized laser beam (CVI) through a computer-generated phase diffractive optical element. The implementation of diffractive optical elements on a spatial light modulator device enabled us to adjust in real time the separation distance between the traps.[27]

A suspension of microbubbles of an experimental phospholipid-coated ultrasound contrast agent (BR-14, Bracco Research S. A.) was injected in a chamber enclosed by two optically clear polystyrene matrix membranes (Opticell™, Thermo Fisher Scientific), which ensure high acoustic transmission. We selected pairs of bubbles with a size close to the resonant size for the frequency of the driving ultrasound, set the initial distance between the centers, and positioned them away from the wall using a micropositioning stage. The chamber was coupled to a single-frequency unfocused ultrasound transducer (Panametrics) by immersion in a water bath. An eight-cycle 2.25 MHz ultrasound pulse with a two-cycle Gaussian taper was produced by a waveform generator (Tabor Electronics) and amplified by a rf power amplifier (ENI) before being transmitted by the transducer. The ultrasound beam overlapped with the focal volume of the microscope objective and its angle of incidence with the optical axis [z in Fig. 1(a)] was 45° so that the acoustic reflection from the objective did not reach the bubbles. Furthermore, the direction of incidence of the beam was orthogonal to the line of centers [x in Fig. 1(a)] to decouple the effects of the primary acoustic radiation force from the mutual interaction through the secondary acoustic radiation force. The sample was illuminated from below and the same microscope objective that was used to focus the optical traps was used to produce a top view transmission image, in conjunction with a $2\times$ magnifier. The ultrahigh speed digital camera Brandaris 128 (Ref. 28) recorded the dynamics near 15×10^6 frames/s, corresponding to a temporal resolution under 70 ns.

Figure 1(b) shows 28 frames extracted from the movie of two microbubbles undergoing radial pulsations and experiencing mutual attraction (enhanced online). The marks in the first and last frames indicate the initial positions of the bubble centers. The bubbles remain spherical during the radial pulsations; we discard the experiments where the bubbles significantly deviate from spherical symmetry. To prevent optical forces from interfering with the dynamics, the laser was briefly blocked during the recording, even though the magnitude of the optical force in the horizontal plane ($\sim 10^{-11}$ N) is four orders of magnitude smaller than the secondary acoustic radiation force we typically measure.

The radius and position as a function of time are extracted from the 128 frames of each recording, using the minimum cost tracking algorithm described in Ref. 29. The optical resolution is 100 nm/pixel; image analysis results in subpixel resolution on the extracted quantities, with a typical accuracy of 30–40 nm for the radius and 70–80 nm for the distance. The pattern of rings generated in the image plane by the Mie scattering of light transmitted by a bubble[30] introduces an experimental uncertainty in setting the in-focus position of a bubble. This ultimately leads to a systematic uncertainty in the determination of the initial bubble radius for each experimental run, and the edge detected through the minimum cost algorithm may not correspond to the correct radius. By conducting a series of control experiments where the focus of the image was varied, we estimated a maximum systematic uncertainty of 10%.

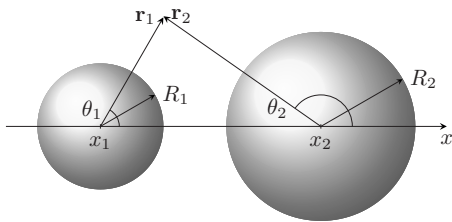The radius- and distance-time curves obtained from im-

FIG. 2. System of coordinates. R_i $(i=1,2)$ is the radius of bubble i and x_i is its position on the line of centers x. $\mathbf{r}_i$ denotes the position of a fluid element relative to bubble i.

age tracking were resampled using a cubic interpolation and filtered using a low-pass filter to remove high-frequency noise. The frequency components of the noise close to the frequency of oscillations cannot be removed by filtering. Therefore, we impose the radius before and after oscillations to be equal to the resting radius, or else the residual noise would give rise to an apparent acoustic radiation force. The maximum difference between the processed data and the measured data points is less than 3%. This is taken as the maximum error on the radius and distance data, and is used to estimate the error on the derived quantities. From the resampled and filtered data we compute the radial and translational velocities and accelerations.

IV. HYDRODYNAMIC MODEL

The system of coordinates is shown in Fig. 2. We take x along the line of centers of the two bubbles with radii R_1 and R_2; the distance between the bubbles is $d=x_2-x_1$. Buoyancy and the primary radiation force act along a direction orthogonal to x and do not affect the translation in the x direction. From conservation of momentum one has the force balance in the x direction for a bubble of radius R:

$$0 = \rho\frac{4}{3}\pi R^3\frac{Du}{Dt} - \frac{1}{2}\rho\frac{d}{dt}\left(\frac{4}{3}\pi R^3 U\right) - 6\pi\eta RU$$
$$- 6\pi\rho\sqrt{\frac{\nu}{\pi}}\int_0^t \frac{d\tau}{\sqrt{\int_\tau^t R(s)^{-2}ds}}\frac{d(RU)}{d\tau}$$
$$= F_G + F_A + F_{QS} + F_H. \tag{1}$$

$U=\dot{x}-u$ is the velocity of the bubble relative to the fluid and $\dot{x}$ is the velocity of the bubble relative to the laboratory frame, with the dot representing differentiation with respect to time. d/dt is the time derivative on the particle trajectory, u is the velocity of the fluid, initially quiescent, generated by the dynamics of the neighboring bubble, and Du/dt is evaluated on the fluid trajectory.

The first term in the right hand side is the force due to the acceleration imparted to the fluid by the neighboring bubble, i.e., the radiation pressure F_G due to the secondary ultrasound wave emitted by a pulsating bubble, the pressure gradient being $\partial p/\partial x=-\rho Du/Dt$; if convective effects are negligible, as is the case here, it reduces to $\partial p/\partial x=-\rho\partial u/\partial t$. The second term is the added mass force F_A on a sphere, which is independent of the boundary condition and of the Reynolds number.[9] Note that since R is time dependent, the added mass force is $F_A=-1/2\rho d/dt(4/3\pi R^3 U)$

$=-\pi\rho(2/3R^3\dot{U}+2R^2\dot{R}U)$. The third term, F_{QS}, accounts for the quasisteady component of the viscous force and the last term for the unsteady component through the history force, F_H. A boundary condition of no slip is assumed at the bubble interface, which is fully immobilized by the layer of surfactant molecules. The quasisteady drag only depends on the instantaneous values of $R(t)$ and $U(t)$. The modification of the kernel of the history integral that accounts for time-dependent radius effects was first introduced by Magnaudet and Legendre[7] for bubbles with shear-free boundary condition and subsequently extended by Takemura and Magnaudet[14] to the case of bubbles that obey a no-slip condition. The integral is evaluated from the time $t=0$ when the bubbles start oscillating. For $t<0$ the velocity of the bubbles is zero, and so is the integral for $-\infty<t<0$. The velocity of the fluid generated by bubble j is evaluated at the center of bubble i $(i,j=1,2,\ i\neq j)$, assuming that the other bubble is absent and that the flow is spatially uniform. The frequency of insonation $f=2.25$ MHz corresponds to a boundary layer of thickness $\delta\sim300$ nm, and in this study we only consider bubbles of radius $R\sim2$ μm. When the viscous boundary layer on the bubble is small with respect to the radius ($\delta\ll R$ or $\omega R^2>\nu$), as is the case here, we may use inviscid theory for determining the flow velocity outside the boundary layer. A pulsating and translating bubble generates a fluid velocity at distance r whose potential has a contribution from a source of strength q, $\Phi_s=-q/4\pi r$, due to the radial pulsations, with the kinematic boundary condition that the velocity at $r=R$ equals $\dot{R}$, and a contribution from a dipole of strength p, $\Phi_p=-p\cos\theta/4\pi r^2$, due to the translation, with p given by the boundary condition that the velocity at $r=R$ is equal to $\dot{x}$. The fluid velocity u is the sum of the two velocities $u=u_r+u_t=\dot{R}\cos\theta R^2/r^2+\dot{x}R^3/r^3(\theta=0,\ \pi)$. If the distance between the bubbles becomes small, the assumption of uniform flow breaks down. In addition, if the wall-to-wall distance between the bubbles becomes comparable with the thickness of the boundary layer, $d-(R_1+R_2)\sim2\delta$, a description of the viscous dissipation in the boundary layer becomes necessary. We limit ourselves to the case $d-(R_1+R_2)\gg2\delta$.

By substituting in Eq. (1) for bubble i the fluid velocity generated by bubble j and retaining terms up to order 3 in R/d, we obtain two coupled equations of motion, identical to this order of accuracy to those obtained by other authors using a Lagrangian formalism.[31–33] The difference with previous models is in the terms that account for viscous effects since only shear-free bubbles were considered before.

The resulting equation of motion describes the translation of a no-slip bubble for a given radial dynamics. The radial dynamics can be modeled through two coupled Rayleigh–Plesset-type equations[31–33] coupled to the translation equations. For coated bubbles this would introduce at least two fitting parameters[16–19] to describe the viscoelastic properties of the coating. For most coating materials the parameters are not known with satisfactory accuracy and may depend on the dilatational rate.[29] Therefore, we use experimental values of R_1, R_2, and their derivatives as time-dependent coefficients.

The numerical integration of the history force was
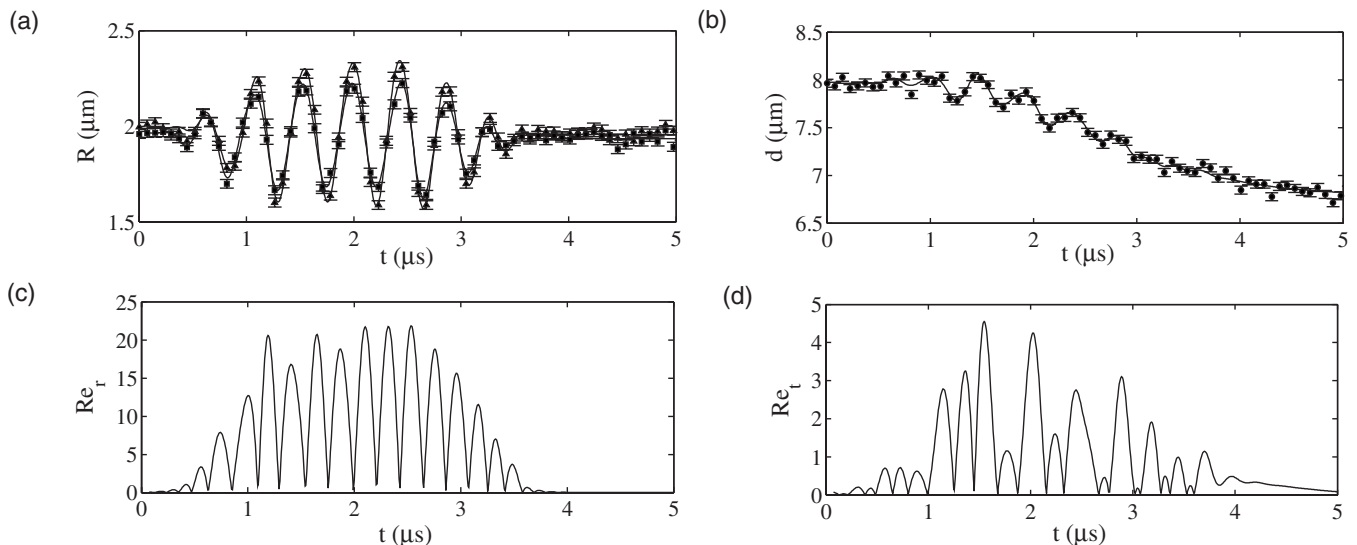
(a)

(b)

(c)

(d)

FIG. 3. (a) Time evolution of the radii obtained by image tracking. The solid symbols represent experimental data points and the lines represent the resampled and filtered radius-time curves. The bubbles oscillate in phase and have relative radial excursions $\Delta R/R_0 \sim 0.3$. (b) Time evolution of the distance between the centers, $d = x_2 - x_1$. The solid symbols represent experimental data points and the line represents the resampled and filtered distance-time curve. [(c) and (d)] Time evolution of the Reynolds numbers computed from the experimental radial and translational dynamics. Only the values for bubble 1 are plotted for clarity. The radial Reynolds number $\mathrm{Re}_r = R|\dot{R}|/\nu$ is below 25 with a time average $\langle \mathrm{Re}_r \rangle \approx 3$. The translational Reynolds number $\mathrm{Re}_t = R|U|/\nu$ is below 5 with a time average $\langle \mathrm{Re}_t \rangle \approx 0.5$.

treated in an approximate fashion to handle the singularity at $\tau = t$ in the kernel of the history integral $\int_0^t d\tau [\int_\tau^t R(s)^{-2} ds]^{-1/2} d(RU)/d\tau$. The integral in the interval $[0, t-dt]$ can be evaluated using standard numerical schemes. By defining the nonlinear mapping $\theta = \int_0^\tau R(s)^{-2} ds$, we write the integral near the singularity as $\int_{\theta(t-dt)}^{\theta(t)} d\theta [\theta(t) - \theta(t-dt)]^{-1/2} d(RU)/d\theta$. Since in our experiments $d(RU)/d\theta$ varies slowly near the singularity, it can be taken as constant over the interval $[\theta(t-dt), \theta(t)]$ and the resulting integral can be evaluated analytically. We tested our approximation against the numerical scheme proposed by Chung,[34] which is commonly used to compute the history integral,[14,35] and found the results to agree to within 0.5%.

V. RESULTS AND DISCUSSION

Figures 3(a) and 3(b) show the time evolution of the radius of the two bubbles and the distance d between their centers. The radial pulsations are in phase with a relative radial excursion $\Delta R/R_0 < 0.3$. The positions of the centers display small translational oscillations (typical amplitude of 200–300 nm) with the same frequency as the radial pulsations, around a position that slowly drifts, resulting in the net attraction expected for bubbles pulsating in phase. When the external forcing is turned off and the radial pulsations have damped out ($t \approx 3.6~\mu$s), the bubbles decelerate subject only to viscous drag. Figures 3(c) and 3(d) show the time evolution of the Reynolds numbers $\mathrm{Re}_r = R|\dot{R}|/\nu$ for the radial dynamics and $\mathrm{Re}_t = R|U|/\nu$ for the translation. The values of the Reynolds numbers during the motion are below 5 for the translation and below 25 for the radial dynamics. The time averages are $\langle \mathrm{Re}_t \rangle \approx 0.5$ and $\langle \mathrm{Re}_r \rangle \approx 3$, respectively. Therefore, we hypothesize that high-Re effects can be neglected in the translational dynamics, an assumption that is confirmed a

posteriori. We also expect that effects due to the time-dependent radius not significantly influence the transport of vorticity but we use the version of the history force for a bubble with time-dependent radius for consistency.

Following Takemura and Magnaudet,[14] we begin our analysis by determining the values of $F_A(t)$, $F_G(t)$, $F_{QS}(t)$, and $F_H(t)$ from the experimental values of $R_1(t)$, $R_2(t)$, $d(t)$, and their derivatives. We can then test the expression for the viscous force $F_{QS} + F_H$ against the value deduced from the force balance, $F_{QS} + F_H = -(F_A + F_G)$. The comparison is shown in Fig. 4. The value of the viscous force determined from experiment is indicated by the dashed line. The error is calculated from the uncertainties on radius and distance and is shown for the set of points that correspond to data points from the experiment. The solid line shows that the zero-Re expression for $F_{QS} + F_H$ shown in Eq. (1) gives a good prediction of the viscous force. The value of F_{QS} is also plotted
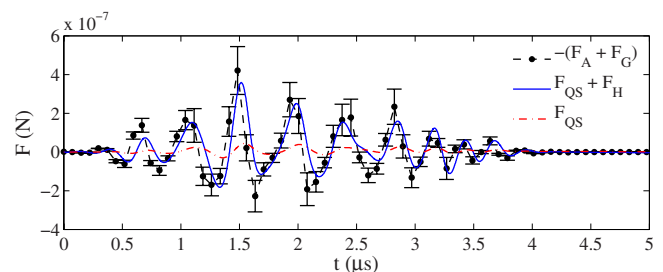

FIG. 4. (Color online) Comparison of models for the viscous force. The values are computed for one bubble from the experimental values of the radius and position and their derivatives. Dashed line: experimental value from the force balance $-(F_A + F_G)$. The solid symbols show the values corresponding to the experimental data points. Solid line: model including quasisteady drag and history force $F_{QS} + F_H$. Dashed-dotted line: a model including only quasisteady drag F_{QS}, neglecting history force, largely underestimates viscous dissipation.
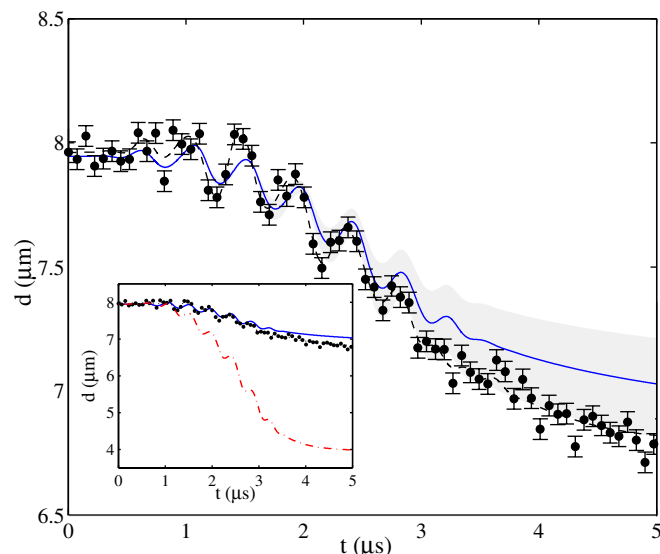
FIG. 5. (Color online) Time evolution of the distance between the centers of the bubbles. Dashed line: experimental value (after resampling and filtering). The solid symbols are the measured data points. Solid line: prediction using the model including history force and quasisteady drag, $F_{QS}+F_H$. The shaded area represents the tolerance ($\pm5\%$) on the prediction due to the systematic experimental uncertainty on the resting radius of a bubble. Inset: comparison of the model including only the quasisteady drag F_{QS} (dashed-dotted line) with the model including history force, $F_{QS}+F_H$ (solid line).

(dashed-dotted line) to emphasize how neglecting the history force would result in a large underestimation of the total viscous force.

Since the governing equations can be linearized if convective effects are negligible, the velocity can be decomposed into its quasisteady and oscillatory components. The oscillatory component experiences an increased viscous dissipation since the vorticity generated at the bubble surface does not diffuse away during one period of oscillation and remains confined to the viscous boundary layer of thickness $\delta\sim\sqrt{\nu/\omega}$. The drag force experienced by an oscillating sphere can be estimated, in the high-frequency limit, as $6\pi\eta(1+R/\delta)RU$.[4] In the range of parameters of our experiments, the drag on the oscillatory component of the velocity is increased by a factor $(1+R/\delta)\sim5$ compared to the quasisteady value $6\pi\eta RU$. The Basset expression for the history force is only strictly valid at zero Reynolds number, or for an oscillatory motion. The main limitation in the applicability of this expression to the present case is probably the $\tau^{-1/2}$ time decay, which was observed to be too slow for a particle accelerating from rest[36] and is not strictly valid for the quasisteady component of the velocity.

We now proceed to test the performance of the model by integrating the equations of motion and predicting the displacement of the bubbles. The experimental values of $R_1(t)$, $R_2(t)$, and their derivatives are substituted in the equations of motion as time-dependent coefficients, and the equations are integrated numerically to obtain the time evolution of $x_1(t)$ and $x_2(t)$. The agreement between the predicted displacement and the experiment is fully satisfactory, as shown in Fig. 5. The comparison with the result obtained by neglecting the history force (inset) emphasizes again how crucial the influ-

ence of this force is for coated bubbles as opposed to shear-free bubbles. As described in Sec. III, for each experimental run the extracted bubble radii can differ from the true radii due to the systematic uncertainty in the imaging. To test the robustness of our findings in this respect, we compute the numerical solution for two limiting cases, $R\pm5\%$. The solution corresponding to the true radii R_1 and R_2 then lies in the shaded area in Fig. 5. The prediction remains highly satisfactory and the model can be used to predict the low-Re translation of coated bubbles of known radius due to acoustic radiation pressure.

VI. SUMMARY AND CONCLUSIONS

We performed a time-resolved study of the translation of coated microbubbles propelled by ultrasound radiation pressure in a range of parameters that is relevant for medical ultrasound imaging. By positioning the bubbles with optical tweezers we were able to exclude the influence of confining geometries and to unambiguously identify the contributions of the several hydrodynamic forces acting on the bubbles. The use of an ultrahigh speed camera operated near 15×10^6 frames/s ensured the required temporal resolution to characterize the unsteady translation of the bubbles. We developed a point-particle model to describe the translation of bubbles subject to secondary radiation pressure due to a neighboring pulsating bubble and found that the inclusion of the history force is crucial for a correct description of the unsteady motion of coated microbubbles. Neglecting this force results in a large underestimation of the viscous dissipation. This can be understood from the fact that the translational velocity has an oscillatory component, which experiences an increased dissipation due to the oscillatory boundary layer that develops around the bubble.

One of the limits of applicability of this model is that the bubbles should be far enough from each other so that the approximation of uniform flow holds and dissipative effects in the boundary layer are unimportant $[d-(R_1+R_2)\gg2\delta]$. Furthermore we restricted ourselves to the case of spherical bubbles, an approximation that breaks down when the bubbles get too close. For longer insonation pulses the bubbles are often observed to lose their spherical symmetry, with nonspherical oscillations arising as a parametric instability.[37] Viscous effects are then more difficult to account for.[38]

[1] M. Brenner, S. Hilgenfeldt, and D. Lohse, "Single-bubble sonoluminescence," Rev. Mod. Phys. **74**, 425 (2002).

[2] L. A. Crum and A. I. Eller, "Motion of bubbles in a stationary sound field," J. Acoust. Soc. Am. **48**, 181 (1970).

[3] L. A. Crum, "Bjerknes forces on bubbles in a stationary sound field," J. Acoust. Soc. Am. **57**, 1363 (1975).

[4] L. D. Landau and E. M. Lifshitz, *Fluid Mechanics*, 2nd ed. (Pergamon, New York, 1987).

[5] H. A. Oğuz and A. Prosperetti, "A generalization of the impulse and virial theorems with an application to bubble oscillations," J. Fluid Mech. **218**, 143 (1990).

[6] A. J. Reddy and A. J. Szery, "Coupled dynamics of translation and collapse of acoustically driven microbubbles," J. Acoust. Soc. Am. **112**, 1346 (2002).

[7] J. Magnaudet and D. Legendre, "The viscous drag force on a spherical bubble with time-dependent radius," Phys. Fluids **10**, 550 (1998).

[8] R. Toegel, S. Luther, and D. Lohse, "Viscosity destabilizes sonoluminescing bubbles," Phys. Rev. Lett. **96**, 114301 (2006).

[9] J. Magnaudet and I. Eames, "The motion of high-Reynolds-number bubbles in inhomogeneous flows," Annu. Rev. Fluid Mech. **32**, 659 (2000).

[10] V. G. Levich, *Physicochemical Hydrodynamics* (Prentice-Hall, Englewood Cliffs, 1962).

[11] A. Basset, *A Treatise on Hydrodynamics* (Deighton Bell, London, 1888), Vol. 2.

[12] G. G. Stokes, "On the effect of the internal friction of fluids on the motion of pendulums," Trans. Cambridge Philos. Soc. **9**, 8 (1851).

[13] R. Mei, "Flow due to an oscillating sphere and an expression for unsteady drag on the sphere at finite Reynolds number," J. Fluid Mech. **270**, 133 (1994).

[14] F. Takemura and J. Magnaudet, "The history force on a rapidly shrinking bubble rising at finite Reynolds number," Phys. Fluids **16**, 3247 (2004).

[15] B. B. Goldberg, J. Raichlen, and F. Forsberg, *Ultrasound Contrast Agents: Basic Principles and Clinical Applications*, 2nd ed. (Dunitz, London, 2001).

[16] N. de Jong, R. Cornet, and C. T. Lancée, "Higher harmonics of vibrating gas-filled microspheres. Part one: Simulations," Ultrasonics **32**, 447 (1994).

[17] C. C. Church, "The effects of an elastic solid surface layer on the radial pulsations of gas bubbles," J. Acoust. Soc. Am. **97**, 1510 (1995).

[18] K. Sarkar, W. T. Shi, D. Chatterjee, and F. Forsberg, "Characterization of ultrasound contrast microbubbles using *in vitro* experiments and viscous and viscoelastic interface models for encapsulation," J. Acoust. Soc. Am. **118**, 539 (2005).

[19] P. Marmottant, S. M. van der Meer, M. Emmer, M. Versluis, N. de Jong, S. Hilgenfeldt, and D. Lohse, "A model for large amplitude oscillations of coated bubbles accounting for buckling and rupture," J. Acoust. Soc. Am. **118**, 3499 (2005).

[20] J. R. Lindner, "Microbubbles in medical imaging: Current applications and future directions," Nat. Rev. Drug Discovery **3**, 527 (2004).

[21] A. L. Klibanov, "Microbubble contrast agents: Targeted ultrasound imaging and ultrasound-assisted drug-delivery applications," Invest. Radiol. **41**, 354 (2006).

[22] S. P. Qin, C. F. Caskey, and K. W. Ferrara, "Ultrasound contrast microbubbles in imaging and therapy: Physical principles and engineering," Phys. Med. Biol. **54**, R27 (2009).

[23] P. A. Dayton, J. S. Allen, and K. W. Ferrara, "The magnitude of radiation force on ultrasound contrast agents," J. Acoust. Soc. Am. **112**, 2183 (2002).

[24] J. Happel and H. Brenner, *Low Reynolds Number Hydrodynamics* (Kluwer Academic, Dordrecht, 1983).

[25] V. Garbin, D. Cojoc, E. Ferrari, E. Di Fabrizio, M. L. J. Overvelde, S. M. van der Meer, N. de Jong, D. Lohse, and M. Versluis, "Changes in microbubble dynamics near a boundary revealed by combined optical micromanipulation and high speed imaging," Appl. Phys. Lett. **90**, 114103 (2007).

[26] B. T. Unger and P. L. Marston, "Optical levitation of bubbles in water by the radiation pressure of a laser beam: An acoustically quiet levitator," J. Acoust. Soc. Am. **83**, 970 (1988).

[27] V. Garbin, D. Cojoc, E. Ferrari, R. Z. Proietti, S. Cabrini, and E. Di Fabrizio, "Optical micro-manipulation using Laguerre–Gaussian beams," Jpn. J. Appl. Phys., Part 1 **44**, 5773 (2005).

[28] C. T. Chin, C. Lancée, J. Borsboom, F. Mastik, M. E. Frijlink, N. de Jong, M. Versluis, and D. Lohse, "Brandaris 128: A digital 25 million frames per second camera with 128 highly sensitive frames," Rev. Sci. Instrum. **74**, 5026 (2003).

[29] S. M. van der Meer, B. Dollet, M. M. Voormolen, C. T. Chin, A. Bouakaz, N. de Jong, M. Versluis, and D. Lohse, "Microbubble spectroscopy of ultrasound contrast agents," J. Acoust. Soc. Am. **121**, 648 (2007).

[30] C. F. Bohren and D. R. Huffman, *Absorption and Scattering of Light by Small Particles* (Wiley, New York, 1983).

[31] A. A. Doinikov, "Translational motion of two interacting bubbles in a strong acoustic field," Phys. Rev. E **64**, 026301 (2001).

[32] A. Harkin, T. J. Kaper, and A. Nadim, "Coupled pulsation and translation of two gas bubbles in a liquid," J. Fluid Mech. **445**, 377 (2001).

[33] Y. A. Ilinskii, M. F. Hamilton, and E. A. Zabolotskaya, "Bubble interaction dynamics in Lagrangian and Hamiltonian mechanics," J. Acoust. Soc. Am. **121**, 786 (2007).

[34] J. N. Chung, "The motion of particles inside a droplet," Trans. ASME, Ser. C: J. Heat Transfer **104**, 438 (1982).

[35] I. Kim, S. Elgobashi, and W. A. Sirignano, "On the equation for spherical-particle motion: Effect of Reynolds and acceleration numbers," J. Fluid Mech. **367**, 221 (1998).

[36] P. M. Lovalenti and J. F. Brady, "The hydrodynamic force on a rigid particle undergoing arbitrary time-dependent motion at small Reynolds number," J. Fluid Mech. **256**, 561 (1993).

[37] B. Dollet, S. M. van der Meer, V. Garbin, N. de Jong, D. Lohse, and M. Versluis, "Nonspherical oscillations of ultrasound contrast agent microbubbles," Ultrasound Med. Biol. **34**, 1465 (2008).

[38] A. Prosperetti, "Viscous effects on perturbed spherical flows," Q. Appl. Math. **34**, 339 (1977).